Technical University of Denmark

DTU

Bismuth ferrite as low-loss switchable material for plasmonic waveguide modulator

Babicheva, Viktoriia; Zhukovsky, Sergei; Lavrinenko, Andrei

[Link back to DTU Orbit](#)

DTU Library
Technical Information Center of Denmark

Bismuth ferrite as low-loss switchable material for plasmonic waveguide modulator

Viktoriia E. Babicheva,[1,2,*] Sergei V. Zhukovsky,[1,2] and Andrei V. Lavrinenko[1]

[1]*DTU Fotonik, Technical University of Denmark, Oersteds Plads 343, 2800 Kgs. Lyngby, Denmark*
[2]*ITMO University, Kronverkskiy, 49, St. Petersburg 197101, Russia*
[*]*v.babicheva@phoi.ifmo.ru*

Abstract: We propose new designs of plasmonic modulators, which can be used for dynamic signal switching in photonic integrated circuits. We study performance of a plasmonic waveguide modulator with bismuth ferrite as a tunable material. The bismuth ferrite core is sandwiched between metal plates (metal-insulator-metal configuration), which also serve as electrodes. The core changes its refractive index by means of partial in-plane to out-of-plane reorientation of ferroelectric domains in bismuth ferrite under applied voltage. As a result, guided modes change their propagation constant and absorption coefficient, allowing light modulation in both phase and amplitude control schemes. Due to high field confinement between the metal layers, existence of mode cut-offs for certain values of the core thickness, and near-zero material losses in bismuth ferrite, efficient modulation performance is achieved. For the phase control scheme, the π phase shift is provided by a 0.8-µm long device with propagation losses 0.29 dB/µm. For the amplitude control scheme, up to 38 dB/µm extinction ratio with 1.2 dB/µm propagation loss is predicted.

References and links

1. A. V. Zayats, I. I. Smolyaninov, and A. A. Maradudin, "Nano-optics of surface plasmon polaritons," Phys. Rep. **408**(3-4), 131–314 (2005).
2. J. A. Schuller, E. S. Barnard, W. Cai, Y. C. Jun, J. S. White, and M. L. Brongersma, "Plasmonics for extreme light concentration and manipulation," Nat. Mater. **9**(3), 193–204 (2010).
3. D. K. Gramotnev and S. I. Bozhevolnyi, "Plasmonics beyond the diffraction limit," Nat. Photonics **4**(2), 83–91 (2010).
4. V. J. Sorger, R. F. Oulton, R.-M. Ma, and X. Zhang, "Toward integrated plasmonic circuits," MRS Bull. **37**(08), 728–738 (2012).
5. J. A. Dionne, L. A. Sweatlock, H. A. Atwater, and A. Polman, "Plasmon slot waveguides: Towards chip-scale propagation with subwavelength-scale localization," Phys. Rev. B **73**(3), 035407 (2006).
6. Y. Kurokawa and H. T. Miyazaki, "Metal-insulator-metal plasmon nanocavities: Analysis of optical properties," Phys. Rev. B **75**(3), 035411 (2007).
7. A. V. Krasavin and A. V. Zayats, "Photonic signal processing on electronic scales: electro-optical field-effect nanoplasmonic modulator," Phys. Rev. Lett. **109**(5), 053901 (2012).
8. A. Emboras, R. M. Briggs, A. Najar, S. Nambiar, C. Delacour, P. Grosse, E. Augendre, J. M. Fedeli, B. de Salvo, H. A. Atwater, and R. Espiau de Lamaestre, "Efficient coupler between silicon photonic and metal-insulator-silicon-metal plasmonic waveguides," Appl. Phys. Lett. **101**(25), 251117 (2012).
9. S. Ishii, M. Y. Shalaginov, V. E. Babicheva, A. Boltasseva, and A. V. Kildishev, "Plasmonic waveguides cladded by hyperbolic metamaterials," Opt. Lett. **39**(16), 4663–4666 (2014).
10. V. E. Babicheva, M. Y. Shalaginov, S. Ishii, A. Boltasseva, and A. V. Kildishev, "Plasmonic waveguides with hyperbolic multilayer cladding," in preparation.
11. K. F. MacDonald and N. I. Zheludev, "Active plasmonics: current status," Laser Photon. Rev. **4**(4), 562–567 (2010).
12. W. Cai, J. S. White, and M. L. Brongersma, "Compact, high-speed and power-efficient electrooptic plasmonic modulators," Nano Lett. **9**(12), 4403–4411 (2009).
13. J. A. Dionne, K. Diest, L. A. Sweatlock, and H. A. Atwater, "PlasMOStor: a metal-oxide-Si field effect plasmonic modulator," Nano Lett. **9**(2), 897–902 (2009).
14. S. Zhu, G. Q. Lo, and D. L. Kwong, "Theoretical investigation of silicon MOS-type plasmonic slot waveguide based MZI modulators," Opt. Express **18**(26), 27802–27819 (2010).

15. S. Zhu, G. Q. Lo, and D. L. Kwong, "Electro-absorption modulation in horizontal metal-insulator-silicon-insulator-metal nanoplasmonic slot waveguides," Appl. Phys. Lett. **99**(15), 151114 (2011).
16. R. Thomas, Z. Ikonic, and R. W. Kelsall, "Electro-optic metal–insulator–semiconductor–insulator–metal Mach-Zehnder plasmonic modulator," Photon. Nanostructures **10**(1), 183–189 (2012).
17. A. Melikyan, N. Lindenmann, S. Walheim, P. M. Leufke, S. Ulrich, J. Ye, P. Vincze, H. Hahn, T. Schimmel, C. Koos, W. Freude, and J. Leuthold, "Surface plasmon polariton absorption modulator," Opt. Express **19**(9), 8855–8869 (2011).
18. V. E. Babicheva and A. V. Lavrinenko, "Plasmonic modulator optimized by patterning of active layer and tuning permittivity," Opt. Commun. **285**(24), 5500–5507 (2012).
19. V. J. Sorger, N. D. Lanzillotti-Kimura, R.-M. Ma, and X. Zhang, "Ultra-compact silicon nanophotonic modulator with broadband response," Nanophotonics **1**(1), 17–22 (2012).
20. V. E. Babicheva, N. Kinsey, G. V. Naik, M. Ferrera, A. V. Lavrinenko, V. M. Shalaev, and A. Boltasseva, "Towards CMOS-compatible nanophotonics: Ultra-compact modulators using alternative plasmonic materials," Opt. Express **21**(22), 27326–27337 (2013).
21. H. W. H. Lee, G. Papadakis, S. P. Burgos, K. Chander, A. Kriesch, R. Pala, U. Peschel, and H. A. Atwater, "Nanoscale Conducting Oxide PlasMOStor," Nano Lett. (2014), doi.org/10.1021/nl502998z.
22. J. Gosciniak and D. T. H. Tan, "Graphene-based waveguide integrated dielectric-loaded plasmonic electro-absorption modulators," Nanotechnology **24**(18), 185202 (2013).
23. A. Melikyan, L. Alloatti, A. Muslija, D. Hillerkuss, P. C. Schindler, J. Li, R. Palmer, D. Korn, S. Muehlbrandt, D. Van Thourhout, B. Chen, R. Dinu, M. Sommer, C. Koos, M. Kohl, W. Freude, and J. Leuthold, "High-speed plasmonic phase modulators," Nat. Photonics **8**(3), 229–233 (2014).
24. J. Gosciniak and S. I. Bozhevolnyi, "Performance of thermo-optic components based on dielectric-loaded surface plasmon polariton waveguides," Scientific Reports **3**, 1803 (2013).
25. J. Gosciniak, S. I. Bozhevolnyi, T. B. Andersen, V. S. Volkov, J. Kjelstrup-Hansen, L. Markey, and A. Dereux, "Thermo-optic control of dielectric-loaded plasmonic waveguide components," Opt. Express **18**(2), 1207–1216 (2010).
26. A. V. Krasavin, A. V. Zayats, and N. I. Zheludev, "Active control of surface plasmon–polariton waves," J. Opt. A, Pure Appl. Opt. **7**(2), S85–S89 (2005).
27. W. Zhao and Z. Lu, "Nanoplasmonic optical switch based on Ga-Si$_3$N$_4$-Ga waveguide," Opt. Eng. **50**(7), 074002 (2011).
28. L. A. Sweatlock and K. Diest, "Vanadium dioxide based plasmonic modulators," Opt. Express **20**(8), 8700–8709 (2012).
29. B. A. Kruger, A. Joushaghani, and J. K. S. Poon, "Design of electrically driven hybrid vanadium dioxide (VO2) plasmonic switches," Opt. Express **20**(21), 23598–23609 (2012).
30. K. J. A. Ooi, P. Bai, H. S. Chu, and L. K. Ang, "Ultracompact vanadium dioxide dual-mode plasmonic waveguide electroabsorption modulator," Nanophotonics **2**(1), 13–19 (2013).
31. A. Joushaghani, B. A. Kruger, S. Paradis, D. Alain, J. S. Aitchison, and J. K. S. Poon, "Sub-volt broadband hybrid plasmonic-vanadium dioxide switches," Appl. Phys. Lett. **102**(6), 061101 (2013).
32. J. T. Kim, "CMOS-compatible hybrid plasmonic modulator based on vanadium dioxide insulator-metal phase transition," Opt. Lett. **39**(13), 3997–4000 (2014).
33. H. M. G. Wassel, D. Dai, M. Tiwari, J. K. Valamehr, L. Theogarajan, J. Dionne, F. T. Chong, and T. Sherwood, "Opportunities and Challenges of Using Plasmonic Components in Nanophotonic Architectures," IEEE Journal on Emerging and Selected Topics in Circuits and Systems **2**(2), 154–168 (2012).
34. E. Feigenbaum, K. Diest, and H. A. Atwater, "Unity-order index change in transparent conducting oxides at visible frequencies," Nano Lett. **10**(6), 2111–2116 (2010).
35. A. P. Vasudev, J. H. Kang, J. Park, X. Liu, and M. L. Brongersma, "Electro-optical modulation of a silicon waveguide with an "epsilon-near-zero" material," Opt. Express **21**(22), 26387–26397 (2013).
36. Z. Lu, W. Zhao, and K. Shi, "Ultracompact electroabsorption modulators based on tunable epsilon-near-zero-slot waveguides," IEEE Photon. J. **4**(3), 735–740 (2012).
37. V. E. Babicheva, I. V. Kulkova, R. Malureanu, K. Yvind, and A. V. Lavrinenko, "Plasmonic modulator based on gain-assisted metal–semiconductor–metal waveguide," Photon. Nanostructures **10**(4), 389–399 (2012).
38. V. E. Babicheva, R. Malureanu, and A. V. Lavrinenko, "Plasmonic finite-thickness metal-semiconductor-metal waveguide as ultra-compact modulator," Photon. Nanostructures **11**(4), 323–334 (2013).
39. A. Petraru, J. Schubert, M. Schmid, and C. Buchal, "Ferroelectric BaTiO3 thin-film optical waveguide modulators," Appl. Phys. Lett. **81**(8), 1375 (2002).
40. P. Tang, D. J. Towner, T. Hamano, A. L. Meier, and B. W. Wessels, "Electrooptic modulation up to 40 GHz in a barium titanate thin film waveguide modulator," Opt. Express **12**(24), 5962–5967 (2004).
41. P. Tang, D. J. Towner, A. L. Meier, and B. W. Wessels, "Low-voltage, polarization-insensitive, electro-optic modulator based on a polydomain barium titanate thin film," Appl. Phys. Lett. **85**(20), 4615 (2004).
42. P. Tang, A. L. Meier, D. J. Towner, and B. W. Wessels, "BaTiO3 thin-film waveguide modulator with a low voltage-length product at near-infrared wavelengths of 0.98 and 1.55 μm," Opt. Lett. **30**(3), 254–256 (2005).
43. M. J. Dicken, L. A. Sweatlock, D. Pacifici, H. J. Lezec, K. Bhattacharya, and H. A. Atwater, "Electrooptic modulation in thin film barium titanate plasmonic interferometers," Nano Lett. **8**(11), 4048–4052 (2008).
44. S. G. Choi, H. T. Yi, S. W. Cheong, J. N. Hilfiker, R. France, and A. G. Norman, "Optical anisotropy and charge-transfer transition energies in BiFeO3 from 1.0 to 5.5 eV," Phys. Rev. B **83**(10), 100101 (2011).
45. V. E. Babicheva and A. V. Lavrinenko, "Plasmonic modulator based on metal-insulator-metal waveguide with barium titanate core," Photonics Letters of Poland **5**(2), 57–59 (2013).

46. S. H. Chu, D. J. Singh, J. Wang, E.-P. Li, and K. P. Ong, "High optical performance and practicality of active plasmonic devices based on rhombohedral BiFeO3," Laser & Photonics Reviews **6**(5), 684–689 (2012).
47. T. Qu, Y. Song, K. Yang, Y. Huang, S. Wu, Z. Tan, and X. Long, "High performance electro-optic modulator employing a thin BiFeO3 film on Au with absorption resonance," in Optical Interference Coatings, M. Tilsch and D. Ristau, eds., OSA Technical Digest (online) (Optical Society of America, 2013), paper MB.6.
48. I. D. Kim, Y. Avrahami, H. L. Tuller, Y. B. Park, M. J. Dicken, and H. A. Atwater, "Study of orientation effect on nanoscale polarization in BaTiO3 thin films using piezoresponse force microscopy," Appl. Phys. Lett. **86**(19), 192907 (2005).
49. M. J. Dicken, K. Diest, Y. B. Park, and H. A. Atwater, "Growth and optical property characterization of textured barium titanate thin films for photonic applications," J. Cryst. Growth **300**(2), 330–335 (2007).
50. P. B. Johnson and R. W. Christy, "Optical constants of the noble metals," Phys. Rev. B **6**(12), 4370–4379 (1972).
51. I. D. Rukhlenko, M. Premaratne, and G. P. Agrawal, "Guided plasmonic modes of anisotropic slot waveguides," Nanotechnology **23**(44), 444006 (2012).
52. J. Feng, V. S. Siu, A. Roelke, V. Mehta, S. Y. Rhieu, G. T. R. Palmore, and D. Pacifici, "Nanoscale plasmonic interferometers for multispectral, high-throughput biochemical sensing," Nano Lett. **12**(2), 602–609 (2012).
53. Y. Gao, Q. Gan, Z. Xin, X. Cheng, and F. J. Bartoli, "Plasmonic Mach-Zehnder interferometer for ultrasensitive on-chip biosensing," ACS Nano **5**(12), 9836–9844 (2011).
54. Ultra-compact plasmonic waveguide modulators, Ph.D. Thesis, Viktoriia Evgenivna Babicheva, DTU Fotonik, Technical University of Denmark, October 2013.

1. Introduction

Plasmonic structures were shown to have advantages for waveguiding and enhanced light-matter interaction, since utilizing surface plasmon waves at a metal-dielectric interface allows efficient manipulation of light on the subwavelength scale [1–4]. A metal-insulator-metal (MIM) waveguide provides the most compact footprint due to high mode localization within the dielectric core, and consequently efficient interaction between the mode and switchable material placed between metal layers [5–7]. Although detailed characterization of the devices encounters issues because of the small mode size and high insertion losses, it has been shown recently that the efficient coupling from a photonic waveguide to an MIM structure can be realized [8]. Moreover, a few other approaches have been proposed, for example confining light either by thick metal layers or by more specifically designed metamaterials, for instance hyperbolic metamaterials [9,10].

Plasmonic waveguide modulators and switches are of major interest for ultra-compact photonic integrated circuits and have been widely studied for the last several years [11,12]. Potentially promising designs have been proposed based on various tunable materials, such as silicon [13–16], transparent conductive oxides (TCOs) [7,17–21], graphene [22], nonlinear polymers [23], thermo-optic polymers [24,25], gallium nitride [26,27], and vanadium dioxide [28–32]. Some of them were shown to outperform conventional photonic-waveguide-based designs in terms of compactness [19,33].

In general, one can distinguish two classes of tunable materials according to physical mechanisms underlying refractive index control: carrier concentration change (e.g. TCOs and silicon) and nanoscale structural transformations (e.g. gallium and vanadium dioxide). For example, TCOs provide a large change of refractive indexes and can be utilized for fast signal modulation on the order of several terahertz [7,17–21,34–36]. However, they possess high losses, consequently, the modal propagation length is fairly small [17,18]. For loss mitigation, one can implement gain materials and directly control the absorption coefficient [37,38], but such active materials can significantly increase the noise level.

In contrast to carrier concentration change, structural transformations cannot provide such high bit rate, and megahertz operation is expected due to microsecond timescales of the transformations. Nevertheless, refractive index changes that accompany nanoscale material transformations are much higher than those caused by carrier concentration change. In particular, the extinction ratio up to 2.4 dB/μm was demonstrated for a hybrid plasmonic modulator, whose operation principle is based on metal – insulator phase transition in vanadium dioxide [31].

Ferroelectric materials, such as bismuth ferrite ($BiFeO_3$, BFO) or barium titanate ($BaTiO_3$, BTO), possess promising features for optical modulation [39–47]. Under applied voltage, the ferroelectric domains can be partially reoriented from the in-plane orientation (with ordinary

refractive index n_o) to the out-of-plane orientation (with extraordinary index n_e) [48,49]. Thus, the refractive index for a field polarized along one axis can be changed, and control of propagating signal is achieved. Variation of the applied voltage provides a varying degree of domain switching, and thus the required level of propagating signal modulation can be realized. BTO was shown to provide effective performance in photonic thin film modulators [39–42]. Furthermore, its electro-optic properties were used in plasmonic interferometer-based [43] and waveguide-based [45] modulators. However, BFO has higher birefringence with refractive index difference $\Delta n_{BFO} = 0.18$, nearly three times higher than that in BTO. Recently, a strong change of the refractive index in BFO has been demonstrated [44] and proposed for electro-optic modulation [46,47].

Here for the first time, we propose implementation of BFO as switchable material for plasmonic waveguide modulators. We analyze different modulator designs based on MIM waveguide configuration, and compare performance of these modulators. Because of low losses of BFO at telecom wavelengths, one can achieve large phase shifts and high extinction ratio on a sub-micron distance. Specifically, we predict a π phase shift in a low-loss phase modulator only 0.8 μm long, and up to 38 dB/μm extinction ratio in a high-contrast absorption modulator. In Section 2, we analyze dispersion properties of an MIM waveguide with the BFO core. In Section 3, the phase and absorption modulation effect is studied in more details. Section 4 follows with summary and conclusions.

2. Eigenmodes of the waveguide with BFO core

Schematic view of the MIM waveguide with the BFO core is shown in Fig. 1(a). We are interested in modulation at the telecom wavelength, $\lambda_0 = 1.55$ μm, so the metal permittivity is fixed to $\varepsilon_m = -128.7 + 3.44i$ (silver [50],). Plasmonic modes are defined by the equation [51]:

$$\tan h(qd) = -\left(\frac{k_m}{q}\frac{\varepsilon_{zz}}{\varepsilon_m}\right)^{\pm 1} \tag{1}$$

where "±" corresponds to symmetric and antisymmetric modes, respectively; d is the core thickness; ε_{xx} and ε_{zz} are diagonal components of the permittivity tensor of the core material; $q = \sqrt{(\varepsilon_{zz}/\varepsilon_{xx})\beta_0^2 - \varepsilon_{zz}k_0^2}$; $k_m = \sqrt{\beta_0^2 - \varepsilon_m k_0^2}$; $k_0 = 2\pi/\lambda_0$ is the wave number in vacuum; $\beta_0 = \beta + i\alpha$ is the complex propagation constant to be determined. We consider $n_o = 2.83$ and $n_e = 2.65$ [44] and solve the dispersion equation of a three-layer structure. We consider two options for the device off-state as shown in Fig. 1(b): with $\varepsilon_{xx} = n_o^2$ and $\varepsilon_{zz} = n_e^2$ ("x-ordinary", denoted "ox") and with $\varepsilon_{xx} = n_e^2$ and $\varepsilon_{zz} = n_o^2$ ("z-ordinary", denoted "oz"). The imaginary part of ε_{ii} is assumed to be negligibly small at 1.55 μm. Under applied voltage, the domains are reoriented, and both off-states switch to the same on-state (labeled "e") with tensor components equal to $\varepsilon_{xx} = \varepsilon_{zz} = n_e^2$ [Fig. 1(b)]. As was shown previously, MIM waveguides with the high-index core are well described by the two-dimensional approximation (i.e. dispersion equation for the infinitely wide structure) for the waveguide width $w \geq 500$ nm [38]. Thus, we restrict our analysis by the two-dimensional case.
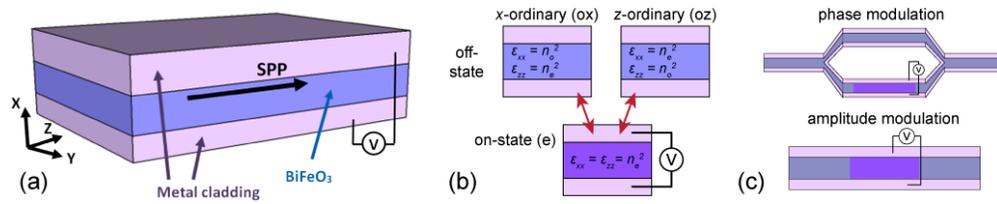
Fig. 1. (a) Schematic view of plasmonic modulator based on metal-insulator-metal waveguide with the switchable BFO core. (b) Illustration of BFO switching in the "*x*-ordinary" and "*z*-ordinary" scenario. (c) Schematics of BFO-based plasmonic switches based on phase or absorption modulation principles.

It was shown that apart from optical properties of constituent materials, the thickness of the core *d* is the primary parameter determining the mode structure of the waveguide. We solve the dispersion Eq. (1) numerically for different core thicknesses *d* = 50…400 nm. As seen in Fig. 2, the structure supports three modes in the considered parameter range: two symmetric (denoted S1 and S2) and one antisymmetric (denoted AS). The results show a significant change of propagation constant β and absorption coefficient α for all three modes during switching between either of the two off-states, (ox) and (oz), and the on-state (e), when the refractive index that corresponds to permittivity tensor component along one of the axes changes from n_o to n_e.

Such difference in the mode indices can allow efficient operation of the device. We see that mode S1 provides the maximum change of β between the off-state (ox) and the on-state [Fig. 2(a)], as well as the lowest losses across the whole range of core thickness variations [Fig. 2(b)]. Thus, this configuration is particularly favourable for a phase modulator in an interferometer-type setup [see Fig. 1(c), top]. On the other hand, the two remaining modes (S2 and AS) feature an abrupt step in the dependence $\alpha(d)$ near the cut-off values of the core thickness, occurring at different *d* for on- vs. off-state [Fig. 2(b)]. These modes are therefore particularly suitable for direct amplitude modulation in a waveguide-type device [Fig. 1(c), bottom], especially when the *z*-ordinary off-state (oz) is used. In the following section, we perform detailed analysis of these regimes.
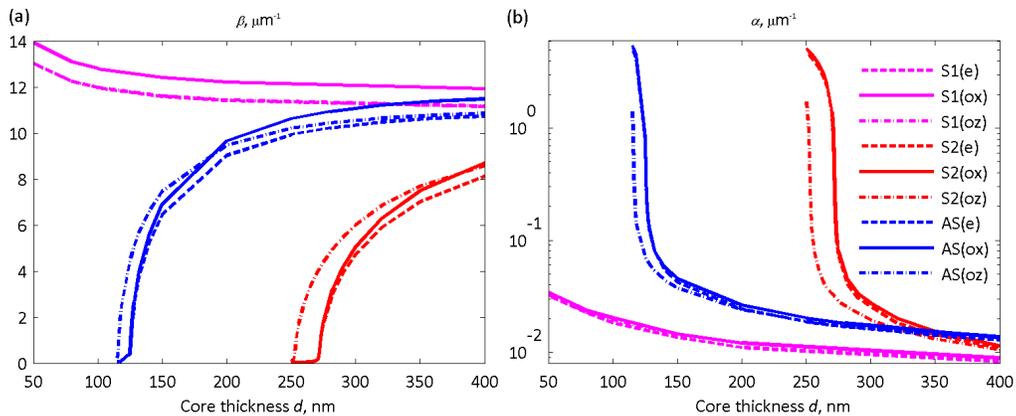

Fig. 2. Propagation constants (a) and absorption coefficients (b) for different modes of MIM waveguide: two symmetric (S1 and S2) and antisymmetric (AS). Labels (ox), (oz), and (e) denote the two off-states (*x*-ordinary and *z*-ordinary) and the on-state, respectively [see Fig. 1(b)]. Legend is the same on both plots.

3. Modulator designs and performance characterization

3.1 Phase-modulation operation

Plasmonic interferometers have being known for a long time and can be used, for instance, in sensing applications [52,53]. Mach-Zehnder interferometers give advantages to utilize phase

shift of the plasmonic waves in two arms and modify resulting transmission through the whole system. The design can be realized by fabrication of multilayer structure, which includes two stacked MIM waveguides as passive and switchable arms [Fig. 1(c), top].

The first symmetric mode S1 possesses the highest β, which varies in the range 11…14 μm^{-1} and corresponds to the values of effective index n_{eff} = 2.7…3.5. The absorption coefficient of this mode is the smallest and has almost no difference between the off- and on-states. Thus, this mode is suitable for signal phase control [Fig. 1(c), top].

We calculated the length required to achieve the π phase shift between the on- and off-states $L_\pi = \pi / (\beta_o - \beta_e)$. The π-shift length is around 4 μm in a broad range of d and decreases with the decrease of core thickness d [Fig. 3(a)]. The propagation losses are 0.08…0.3 dB/μm and on such short L_π length allows relatively high transmission [T_{dB} = $10\log(T_0/T) = 8.68\alpha L_\pi$, Fig. 3(b)].
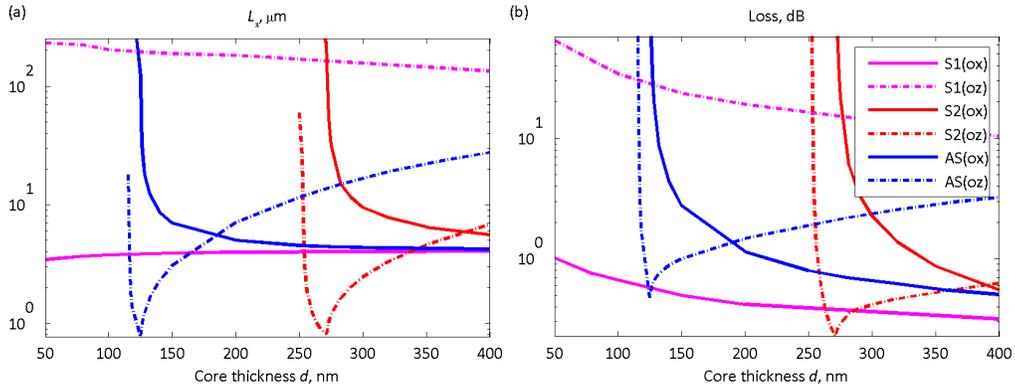

Fig. 3. (a) Device length L_π needed to achieve π phase difference between on- and off-state. (b) Loss in the device with length L_π. The labels (ox) and (oz) correspond to the switching scenarios from the x- and z-ordinary off-state to the on-state [see Fig. 1(b)]. Legend is the same on both plots.

Thus, the phase control can be put into practice via the Mach-Zehnder interferometer with the device length down to 4 μm. The operation bandwidth is large since the effect of mode index change is essentially non-resonant, as indicated by near-flat purple lines in Fig. 3(a), and since BFO has nearly flat dispersion [44].

Comparing BTO and BFO, we reiterate that the latter has three times higher birefringence (Δn_{BFO} = 0.18 versus Δn_{BTO} = 0.05). Consequently, using BFO allows to achieve π phase change on a shorter device length. It was shown that a similarly designed BTO-based modulator operating with the S1 mode achieves a π phase change with a 12…15 μm length device [45] compared with 4 μm in the present device.

It was also shown in Ref [45]. that substituting silver by gold, which is a more practical plasmonic material but has higher losses (ε_{Au} = –115 + 11.3i at λ_0 = 1.55 μm [50]), the propagating constant β of the mode in question is almost unchanged, while the attenuation constant α is increased approximately by four times. Thus, four-time increase of losses in comparison to Fig. 3(b) is expected for the similar device with gold.

On the other hand, when the core thickness varies, the second symmetric S2 and antisymmetric AS modes possess a much more abrupt change. They have very low β and high α for some particular thicknesses, which correspond to the modes exhibiting cut-off (Fig. 2). We can reckon the mode as propagating, when it satisfies the condition $Q = \beta/\alpha > 1$. Thus the mode S2 has cut-off at: $d_{S2}^{(e)} = d_{S2}^{(ox)} = 272$ nm and $d_{S2}^{(oz)} = 253$ nm. Because of the fast pronounced changes near the cut-off thicknesses, the range d = 253…272 nm corresponds to the largest differences between $\beta_{S2}^{(e)}$ and $\beta_{S2}^{(oz)}$. The length required for the π phase shift is reduced to 800 nm [see Fig. 3(a)], and the mode losses are even lower than for S1 [see Fig. 3(b)]. Similar properties are shown by mode AS in the range of thicknesses 116…125 nm.

The propagation losses of these two modes are 0.29 and 0.6 dB/µm. Thus, BFO can be adopted in a low-loss ultra-compact plasmonic modulator.

3.2 Absorption-modulation operation

Another way to implement a plasmonic switch is direct manipulation with absorption coefficient α. Both modes S2 and AS provide such possibility due to cut-off discussed above [see Fig. 2(b)]. Because of losses in plasmonic waveguides, one can define the figure of merit (FoM) of the device as (see e.g [54].)

$$F = (\alpha_e - \alpha_o) / \alpha_o. \tag{2}$$

Both modes have high FoMs in the cut-off region, where there is an abrupt α change [Fig. 4(a)].

For the symmetric mode S2, the FoM value can reach 67. At this point, the extinction ratio $E = 8.68(\alpha_e - \alpha_o) = 20$ dB/µm, and consequently 3 dB switch can be realized on the 150 nm distance. Corresponding propagation length $z = 1/(2\alpha_o)$ is 12 µm [Fig. 4(b)]. For the asymmetric mode AS, the device characteristics are also prominent: FoM up to 29, extinction ratio $E = 28$ dB/µm (allowing a 3 dB switch on 107 nm), and propagation length $z_{AS} = 3.5$ µm [Fig. 4(b)]. Even though there are disadvantages associated with increased absorption, direct modulation of absorption coefficient allows for geometrically simpler and more compact modulator designs than phase modulation.

For all considered designs, modes are strongly localized within the core, and efficient coupling from a photonic waveguide can be realized to launch the symmetric mode [8]. If it is specially required by the design, launching of an asymmetric mode can also be accomplished by coupling to another plasmonic waveguide with already excited asymmetric mode.
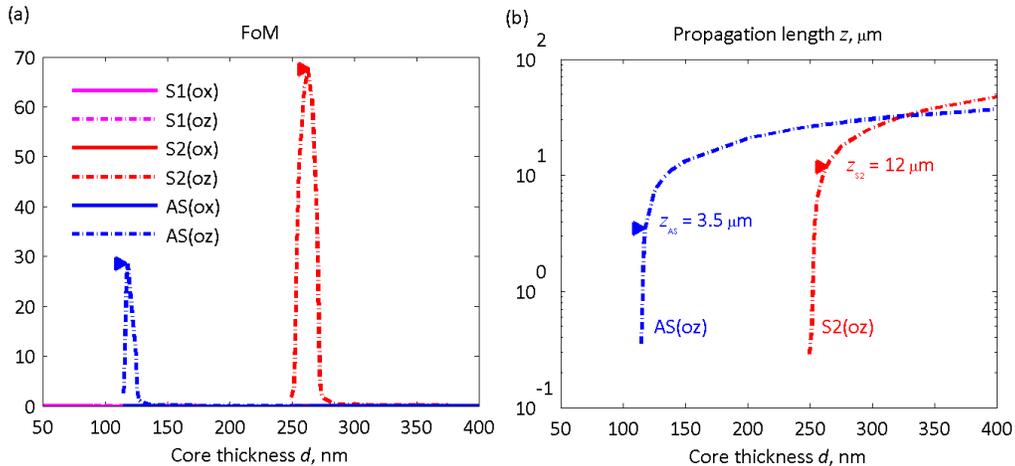

Fig. 4. (a) FoM and (b) propagation length z for the second symmetric (S2) and asymmetric (AS) modes. Triangular marks on (b) correspond to maximum FoM on (a). The first symmetric mode S1 gives nearly zero FoM value.

4. Conclusion

In summary, we studied properties of the MIM plasmonic waveguide with the BFO core, aiming to utilize such a waveguide as a device for an efficient plasmonic modulator. The proposed designs possess the following three advantages.

i) From the material point of view, low losses of BFO do not cause additional attenuation in the waveguide core, and thus do not increase insertion loss of the whole device, in contrast to TCO or vanadium dioxide.

ii) From the design point of view, the MIM configuration allows cut-off of the propagating mode and thus makes it possible to modulate propagation signal by switching it on and off with the metal layers serving as electrodes.

iii) MIM configuration provides high confinement of the mode, and the field does not expand outside waveguide cladding.

The device can be realized in two ways, as shown in Fig. 1(c). On the one hand, signal phase control can be implemented in a Mach-Zehnder interferometer, where device length of 0.8…4 μm is required. Such a compact structure indicates the high potential of BFO-based devices. Moreover, the mode characteristics do not exhibit pronounced changes when the core thickness varies. On the other hand, effective signal amplitude control by direct change of absorption can be realized. In this case a BFO plasmonic modulator can have FoM up to 67 according to Eq. (2), which is comparable with recently reported values for modulators based on a dielectric-loaded plasmonic waveguide with graphene [22]. Meantime, it is much higher than FoMs of previously reported devices based on indium tin oxide, vanadium dioxide, or InGaAsP active layers [18,29,37,38].

Finally, while only fixed-wavelength operation at $\lambda_0 = 1550$ nm was considered, being the most relevant for telecom-range operation, we note that the results can be generalized for broader band operation because of the low losses of BFO (negligible for $\lambda > 1400$ nm [44]) and because of its negligible frequency dispersion around 1550 nm. Specifically, operation with the first symmetric waveguide mode can be broadband as the BFO refractive index is only slightly dispersive at wavelengths close to the telecom range.

Acknowledgments